Earth and Planetary Science Letters 434 (2016) 171–186

Contents lists available at ScienceDirect

Earth and Planetary Science Letters

www.elsevier.com/locate/epsl

Full vector archaeomagnetic records from Anatolia between 2400 and 1350 BCE: Implications for geomagnetic field models and the dating of fires in antiquity

P. Ertepinar [a,*], C.G. Langereis [a], A.J. Biggin [b], L.V. de Groot [a], F. Kulakoğlu [c], S. Omura [d], A. Süel [c]

[a] Paleomagnetic Laboratory Fort Hoofddijk, Department of Earth Sciences, University of Utrecht, Budapestlaan 17, 3584 CD Utrecht, The Netherlands
[b] Geomagnetism Laboratory, Oliver Lodge Laboratories, Department of Earth, Ocean and Ecological Sciences, University of Liverpool, Liverpool L69 7ZE, UK
[c] Department of Archaeology, Faculty of Humanities, Ankara University, Ankara 06100, Turkey
[d] Japanese Institute of Anatolian Archaeology, Çağırkan, Kaman, Kırşehir, Turkey

ARTICLE INFO

Article history:
Received 12 March 2015
Received in revised form 25 October 2015
Accepted 11 November 2015
Available online 8 December 2015
Editor: B. Buffett

Keywords:
archaeomagnetism
archaeointensity
palaeosecular variation
Hittite
Assyrian
Turkey

ABSTRACT

Anatolia, as one of the busiest crossroads of ancient civilizations, provides an ideal platform for archaeomagnetic studies. Previous results from the Middle East have suggested the occurrence of a strong peak in geomagnetic intensity at ~1000 BCE associated with dramatic field strength variations that could require a radical rethinking of geodynamo theory. The behavior of the field in the centuries preceding this peak remains poorly constrained, however. Here we present the results of full-vector archaeomagnetic experiments performed on 18 sets of samples from three archaeological sites belonging to Assyrian Trade Colony and Hittite periods. Associated rock magnetic analyses showed that the major magnetic carrier is magnetite chemically stable up to 700 °C and the magnetic mineral assemblage is composed mostly of non-interacting PSD grains.

The directional results are compared with existing data and with the most recent global geomagnetic field models pfm9k.1b and SHA.DIF.14k. The directions are in remarkably good agreement with SHA.DIF.14k which is based on archaeomagnetic and lava flow data. Together with our earlier results from Anatolia, we triple the existing database of directions for the 700 year long period 2200–1500 BCE, over a large region from Greece to Azerbaijan, and from Moldavia/Ukraine to Egypt.

Three archaeointensity methods: thermal IZZI-Thellier, microwave Thellier and the multi-specimen protocol (MSP) produced virtual axial dipole moment estimates ($9.0–10.9 \times 10^{22}$ Am^2) that are somewhat higher than contemporaneous (regional and global) data and model predictions suggesting that the field was already substantially stronger than today more than 800 years prior to the reported peak. In addition to constraining geomagnetic variability, our data also allow us to assign relative dates to inferred fire events in the Assyrian Trade Colony Period sites. This allows us to conclude that the fire events at the largest site, Kültepe, were not all contemporaneous with one another and with the abandonment of the site as has been previously hypothesized.

1. Introduction

Over the past decade, evidence for a short-lived period of very high geomagnetic intensities in the Levant rapidly accumulated (Ben-Yosef et al., 2009; 2008b; Gallet and al-Maqdissi, 2010; Gallet and Butterlin, 2015; Gallet et al., 2014, 2006, 2008; Gallet and Le Goff, 2006; Genevey et al., 2003; Shaar et al., 2011; Stillinger et al., 2015). At least three studies present reliable paleointensities that exceed twice the current field strength in this region ~1050–850 BCE. The occurrence of extreme geomagnetic field intensity variations during a few decades at most, referred to as *'geomagnetic spike'* (Ben-Yosef et al., 2009) sparked considerable debate: such geomagnetic features are not captured by even the most recent geomagnetic models describing changes in the field (Nilsson et al., 2014; Pavón-Carrasco et al., 2014). Moreover, it was recently shown that current geodynamo theory cannot sustain the existence of this phenomenon (Livermore et al., 2014).

* Corresponding author. Tel.: +31 30 253 1361.
E-mail addresses: pinar@geo.uu.nl (P. Ertepinar), A.Biggin@liverpool.ac.uk (A.J. Biggin), kulakoglu@ankara.edu.tr (F. Kulakoğlu), d.erbisim@jiaa-kaman.org (S. Omura).

http://dx.doi.org/10.1016/j.epsl.2015.11.015
0012-821X/

Most of the available data for this region is derived from archaeological artefacts, such as sherds, copper slag or fired mud-bricks. Their rock magnetic properties are generally favourable, but such samples are often found un-oriented, so they do not provide constraints on directional variations. Only in-situ materials like kilns or burnt mud-brick walls provide the opportunity to obtain reliable palaeodirections; studies reporting these or full vector descriptions of the field are scarce (e.g.: Bucha and Mellaart, 1967; Sarıbudak and Tarling, 1993; Ertepinar et al., 2012). Therefore, directional records for the Levant are supported by less data than the palaeointensity curve for the past millennia – only 30% of the data in GEOMAGIA50 includes directions. Directional data is particularly scarce ∼2200–1500 BCE, part of the Assyrian and Hittite periods in the Levant.

To further constrain the occurrence of the high palaeointensities – and to possibly elucidate their driving force – a full vector record of the geomagnetic field in this area for the past 5 millennia is indispensible. Here, we look at Anatolia as one of the busiest crossroads of ancient civilizations, an ideal platform for archaeomagnetic studies. Here, we present new data from two Assyrian (Kültepe and Kalehöyük) and one Hittite (Şapinuva) Period site. The Assyrian sites and their excavation levels are older, of Middle Bronze Age (2000–1750 BCE). Only one level in Kültepe (KT12) is Early Bronze Age (∼2400 BCE) (Table 1). The Hittite site Şapinuva is of Late Bronze Age, ∼1350 BCE. Our new data triples the available directional information for this particular time interval. Our palaeointensities are obtained by three different and independent methods: thermal IZZI-Thellier experiments, the Microwave Thellier technique, and the Multi-specimen protocol. The credibility of our findings is greatly enhanced if the results of (at least two of) these methods agree. We compare our results to the latest compilations and models of the field, pfm9k.1b (Nilsson et al., 2014) based on both sediment and igneous/archaeomagnetic data, and SHA.DIF.14k (Pavón-Carrasco et al., 2014) based on archaeomagnetic and lava flow data alone.

2. The Bronze Age in Anatolia

In the early second millennium BCE, Anatolia was in the form of city-states where Assyrian merchants came to trade textiles and metals. These merchants sometimes resided in Anatolia which gave the era its name: Assyrian Trade Colony Period. After the trading relations had started, a number of trading centers called *Karum* were established in the major cities of the time. This is also contemporaneous with the earliest writing to appear – inscribed on clay cuneiform tablets. There are more than 20.000 tablets found in Kültepe, 'the trade capital of the period', dating between 1950–1700 BCE. The richness of cultural findings and extensive dendrochronology studies allowed the archaeologists to have a well defined age constraint on the site. This unique combination made Kültepe the reference site for dating the other archaeological sites. The Assyrian Trade Colony Period ended at ∼1685 BCE with the emergence of Hittites in Anatolia (Fig. 1).

Around 1700 BCE, people of unknown origin migrated to Anatolia and united the city states under one central authority, laying the foundations of the Hittite empire centered at Hattusa, which is now a UNESCO World Heritage site. The domination of the Hittites lasted for almost a thousand years and the empire reached its height in the 14th century BCE controlling a large part of Anatolia, the northern Levant and Upper Mesopotamia. The reign started as a kingdom (Old Kingdom, ca. 1650–1500 BCE), then became an Empire between 1400–1200 BCE. After 1180 BCE, the empire disintegrated into several independent city states called Neo-Hittites and completely vanished by the 8th century BCE. The historical documentations of Hittites show a remarkable political and military power as well as a very rich and long lasting culture (Sagona and Zimansky, 2009).

A detailed description per site can be found in the supplementary information (Appendix), here we report the main characteristics and archaeological background of the sites.

Kültepe (KT)

Kültepe, ancient Kaneš, is one of the primary sites of the Assyrian Trade Colony Period, and has served as the point of contact between Assyria and the rest of central Anatolia. It produced the most textual (in cuneiform script) and archaeological evidence. The settlement is composed of two parts; an upper town (the mound) where the palace and the temple were located, and a lower town which contained a large merchant quarter (Kârum). The Kârum of Middle Bronze Age is composed of four levels (I–IV), the youngest having two phases (Ia–Ib). We have sampled 12 sites from levels 1b and II; 2 from the mound and 10 from the Kârum. The levels are well dated by means of dendrochronology (of juniper wood) and tablets (Table 1). One site (KT12) is of Early Bronze age and dated by archaeological findings. It consists of intensely burnt (vitrified) mud-brick. The chronology chart of Assyrian Trade Colony Period sites is given in the appendix (Fig. A1).

From the mound we took 3 sets, from the Kârum part we took 10 sets (Table 1). Oriented cores were drilled from mud-bricks which are usually well heated during the fires, but we also took samples from the foundation stones, here typically ignimbrites from a nearby stratovolcano (Erciyes, near Kayseri) (Fig. A2, Table 1). One of the main puzzles for the archaeologists is the timing and character of the demise of this settlement. By comparing our archaeomagnetic results from different parts of the settlement, we hope to (partly) solve these puzzles. We will argue that this settlement was destroyed (burned) in various stages.

Kalehöyük (KA)

The site Kalehöyük is a medium-sized mound of which the levels have been correlated to the Kültepe-Kârum chronology (Fig. A1). This correlation can be tested by our archaeomagnetic results, and we will argue that may require modification. Archaeomagnetic samples were taken from four structures allegedly belonging to levels Ib (KA1, KA4) and II (KA2) and one older level (KA3) (Fig. A3, Table 1). Here, the foundation stones are granite rather than ignimbrite.

Şapinuva (SPN)

Şapinuva (or Sapinuwa) is a Late Bronze Hittite city (∼1300 BCE) and was one of the major religious and administrative centres and occasional residence of Hittite Kings. Only one site (SPN1) could be sampled; samples were taken from fallen mud-brick blocks of a public building ('Building-A') which is believed to have fallen during the fire that were lying on the sandstone and limestone foundation stones (Fig. A4, Table 1). It is therefore assumed that the mudbricks are *in-situ*.

3. Rock magnetic analyses and results

Room temperature bulk magnetic susceptibilities and thermomagnetic curves were determined for the identification of the magnetic carriers and thermal stability. Based on the preliminary results from these experiments and the quality of the directional results, 9 sites appeared to be suitable for archaeointensity measurements. For these, we additionally performed hysteresis loop, Isothermal Remanent Magnetization (IRM) acquisition and First Order Reversal Curve (FORC) diagram experiments (Roberts et al., 2000).

Low field bulk magnetic susceptibility. Samples were measured with a Kappabridge KLY-2. The results are homogeneous among

Table 1
Archaeomagnetic sites sampled for this study. N is the number of samples and N_{spec} is the total number of samples including sister cores.

Site	Epoch	Corresponding Kültepe-Karum level	Age (BCE)	Dating method	Structure	Material	N	N_{spec}
Şapinuva *(40°16'07"N, 35°14'54"E)*								
SPN1	Late Bronze	–	1350 ± 50	Dendrochronology	Public building	Mud-brick	9	15
Kale Höyük *(39°21'46"N, 33°47'12"E)*								
KA1	Middle Bronze	Kültepe-Karum Ib	1765 ± 65	Archaeological findings	Mud-brick wall	Mud-brick	12	12
KA2	Middle Bronze	Kültepe-Karum II	1892.5 ± 57.5	Archaeological findings	Mud-brick wall and foundation stones	Mud-brick, granite	26	46
KA3	Middle Bronze – Early Bronze transition	–	2000 ± 100	Archaeological findings	Fire place	Granite	9	15
KA4	Middle Bronze	Kültepe-Karum Ib	1765 ± 65	Archaeological findings	Foundation stones	Granite	13	26
Kültepe *(38°51'04"N, 35°38'69"E)*								
KT1	Middle Bronze	Kültepe-Karum Ib	1750 ± 20	Tablets, dendrochronology, C14	Warşama Palace	Mud-brick	25	34
KT2	Middle Bronze	Kültepe-Karum II	1850 ± 20	Tablets, dendrochronology, C14	Güney Palace	Mud-brick	34	54
KT3	Middle Bronze	Kültepe-Karum II	1892.5 ± 57.5	Tablets, dendrochronology	1995 – atelier	Mud-brick	18	18
KT4	Middle Bronze	Kültepe-Karum II	1892.5 ± 57.5	Tablets, dendrochronology	Selim Assur House	Mud-brick, ignimbrite	14	20
KT5	Middle Bronze	Kültepe-Karum II	1892.5 ± 57.5	Tablets, dendrochronology	Uşur-şa-iştar House	Mud-brick, ignimbrite	46	74
KT6	Middle Bronze	Kültepe-Karum Ib	1765 ± 65	Tablets, dendrochronology	House from 2001 archive	Ignimbrite	9	13
KT7	Middle Bronze	Kültepe-Karum Ib	1765 ± 65	Tablets, dendrochronology	House with a mill	Ignimbrite	12	16
KT8	Middle Bronze	Kültepe-Karum II	1892.5 ± 57.5	Tablets, dendrochronology	Ilemma House	Mud-brick, ignimbrite	14	20
KT9	Middle Bronze	Kültepe-Karum Ib	1765 ± 65	Tablets, dendrochronology	House	Ignimbrite	21	34
KT10	Middle Bronze	Kültepe-Karum Ib	1765 ± 65	Tablets, dendrochronology	House	Ignimbrite	7	13
KT11	Middle Bronze	Kültepe-Karum Ib	1765 ± 65	Tablets, dendrochronology	House	Ignimbrite	9	16
KT12	Early Bronze III	–	2400 ± 50	Archaeological findings, C14	Mud-brick wall	Vitrified mud-brick	24	56
KT13	Middle Bronze	Kültepe-Karum II	1892.5 ± 57.5	Tablets, dendrochronology	House	Mud-brick, ignimbrite	21	23

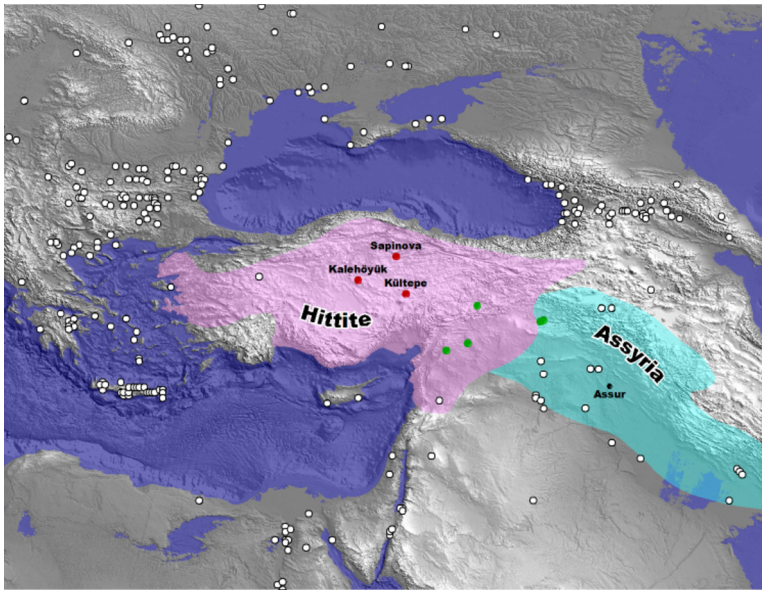

Fig. 1. Map showing the sampling locations (red circles) and the boundaries of Hittite and Assyrian Kingdoms. Green circles are the previously published data from Anatolia (Ertepinar et al., 2012). White circles refer to the locations of data points from GEOMAGIA50v2 (Korhonen et al., 2008) within a circle of ∼1600 km from Kültepe (Kayseri province, 38.85°N and 35.63°E), the approximate center of Turkey – which is used as the reference point. (For interpretation of the references to color in this figure legend, the reader is referred to the web version of this article.)

different rock types and the values range $0.05–35.0 * 10^{-3}$ SI. The results are used to calculate the Koenigsberger Ratio (Q_n) which is an appropriate measure to distinguish whether the samples carry a complete thermoremanent magnetization (TRM). All materials other than the majority of KA granites have Q_n value greater than 1 indicating that TRM strongly dominates, providing a positive stability test (Fig. 2a).

***Thermomagnetic curves* (*Curie balance*).** Measurements were done using a modified horizontal translation type Curie balance that uses a cycling rather then a steady magnetizing field (Mullender et al., 1993). Field settings varied from 50–300 mT to 270–300 mT. Heating and cooling rates were 10 °C/min and experiments were done in air. For all types of materials other than the KT ignimbrites, the heating and cooling curves are essentially reversible indicating that the magnetic minerals are chemically stable until 700 °C (Fig. 2b–g). The mud-brick samples from KA, KT and the granite (KA) and ignimbrite (KT) samples have a single Curie temperature (T_c) at ∼580 °C which is characteristic for magnetite (Fig. 2b–d). The mud-bricks of SPN also have a T_c at ∼580 °C, again pointing to the presence of magnetite as the main carrier, but there is an extra inflection point at ∼350 °C, which could point to some maghemite, or possibly titanomagnetite or Al-substituted magnetite (Fig. 2e). The vitrified mud-bricks from KT12 exhibit an almost reversible curve which shows mainly paramagnetic contribution preventing the identification of any magnetic carrier (Fig. 2f). The curves from some ignimbrites of KT show a difference between heating and cooling curves resulting in irreversible loss in magnetization up to 80% indicating major alteration (Fig. 2g).

Hysteresis loops and FORC diagrams. For the sites that looked promising for archaeointensity measurements, additional rock magnetic properties such as hysteresis loops, IRM acquisition curves and FORC diagrams were investigated, to assess domain state and magnetic stability. From each set 3–5 samples were measured with an alternating gradient force magnetometer. After correction of the paramagnetic and diamagnetic contributions on the hysteresis loops (Fig. 3a) we derived the hysteresis loop parameters (H_c, M_s) while from the IRM acquisition curves (Fig. 3b) we derived the remanence parameters (H_{cr}, M_{sr}). From their ratio's we constructed a Day Plot (Day et al., 1977) to analyse the domain state of the samples. The results of all 29 measurements show that the samples contain only pseudo single domain (PSD) grains (Fig. 3c, Table A1). There is no indication of a high coercivity mineral since all the samples are saturated at or below 200 mT (Fig. 3b).

A FORC diagram is also useful to assess the domain state of magnetic minerals. It additionally gives information about the local interaction fields for an assemblage of magnetic particles (Roberts et al., 2000). Three diagrams from each type of building material are shown in Fig. 3d. The mud-bricks from KA have a symmetrical FORC diagram with a peak distribution centered close to the origin, showing a B_c slightly lower than derived from the hysteresis analysis, with a minor spread along the B_u axis which suggests the presence of small MD or PSD grains with minimal magnetostatic interaction. The FORC distribution of the mud-bricks and vitrified mud-bricks from KT have one closed inner contour with peaks at $B_c = 10$ mT and $B_c = 20$ mT, respectively, consistent with those determined from the corresponding hysteresis loops. Both diagrams have a very narrow contour spreading along the ordinate indicating the assemblages are dominated by non-interacting PSD grains.

Based on the rock magnetic measurements, we decided that all selected sets are suitable for archaeointensity experiments.

4. Methods

To determine the characteristic remanent magnetization direction (ChRM) at least 8 specimens per site were demagnetised (Table 2a) thermally (TH) or with alternating field (AF). The demagnetization was performed with small AF or TH increments (at least 15 steps) up to a maximum of 100 mT or 580 °C. AF demagnetization is carried out after heating the samples to 150 °C to remove possible high coercivity and low T_c minerals, or to remove possible stress in magnetite grains at low temperatures. The demagnetization results were interpreted via orthogonal projection diagrams using an eigenvector approach. The acceptance criteria for maximum angular deviation (MAD) of individual directions and the α_{95} of the means are taken as 10°, but values are typically much lower than that. Figs. 4 and 5 show representative exam-

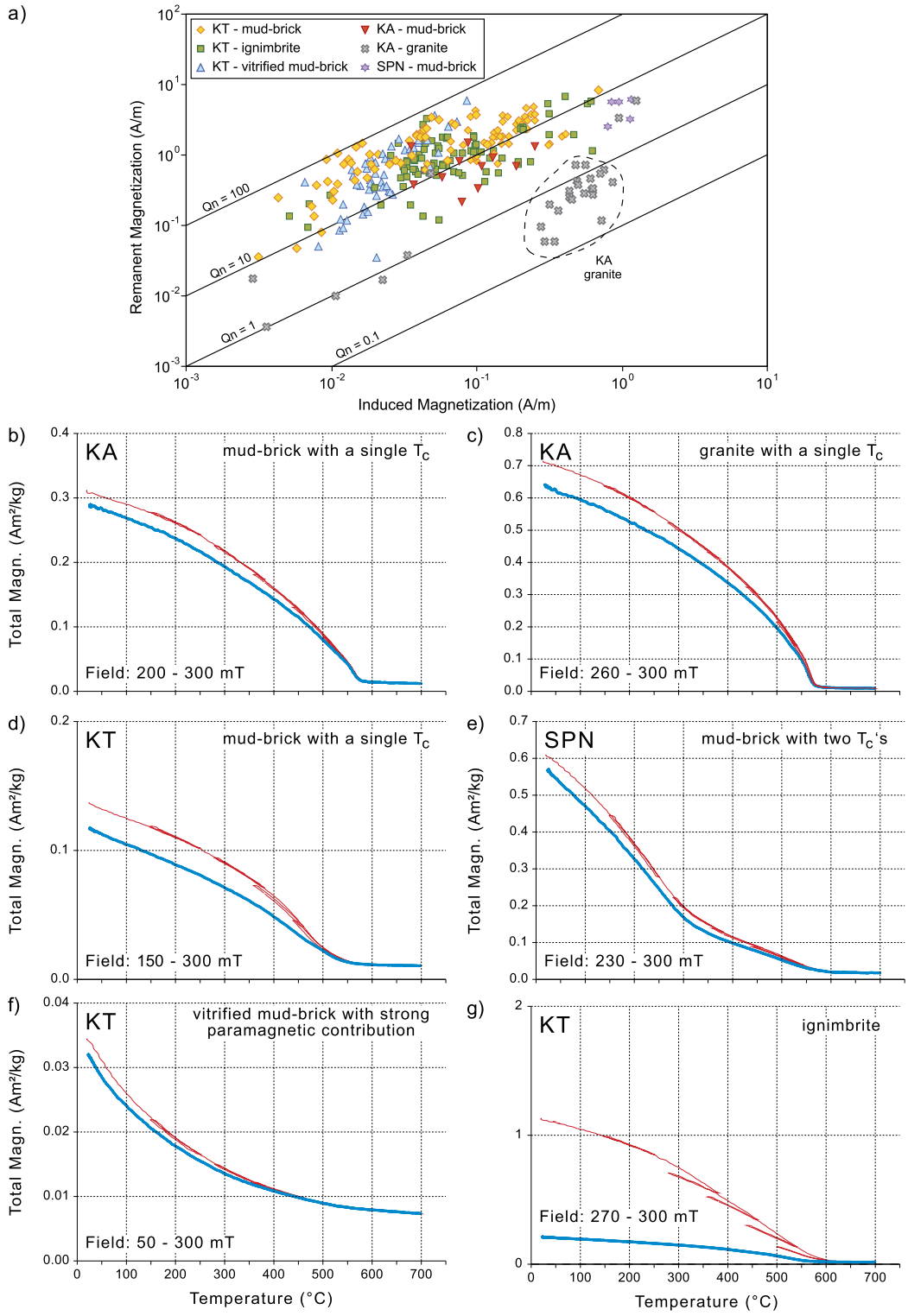

Fig. 2. (a) The Koenigsberger ratio (Q_n) of remanent versus induced magnetization. The black lines show the Koenigsberger ratio isolines. For the materials other than granites of KA, the values cluster at $10 < Q_n < 100$ providing a positive stability test. (b–g) Representative Curie curves for different groups of magnetic composition or behavior: (b) mud-brick and (c) granite sample from KA, (d) mud-brick sample from KT all showing ideal magnetite magnetization with a single Curie point at ~580 °C; (e) mud-brick sample from SPN with T_c at ~580 °C pointing to the presence of magnetite as the main magnetic carrier; the extra inflexion in both curves indicates a secondary carrier (at ~350 °C) which could indicate possible presence of maghemite, titanomagnetite or Al substituted magnetite; (f) Vitrified mud-bricks from KT12 that exhibit an almost reversible Curie balance curve with strong paramagnetic contribution; (g) ignimbrite showing a major difference between heating and cooling curves resulting in irreversible loss in magnetization up to 80%.

ples of demagnetization diagrams for each type of material and the ChRM directions of each set.

For the paleointensity measurements, we adopted three protocols. We emphasized the TT experiments, together with a fair number of MW experiments. In addition, if specimens were still available, we added a small number of multi-specimen experiments (Dekkers and Böhnel, 2006) corrected for domain state according to Fabian and Leonhardt (2010). Fig. 6a shows representa-

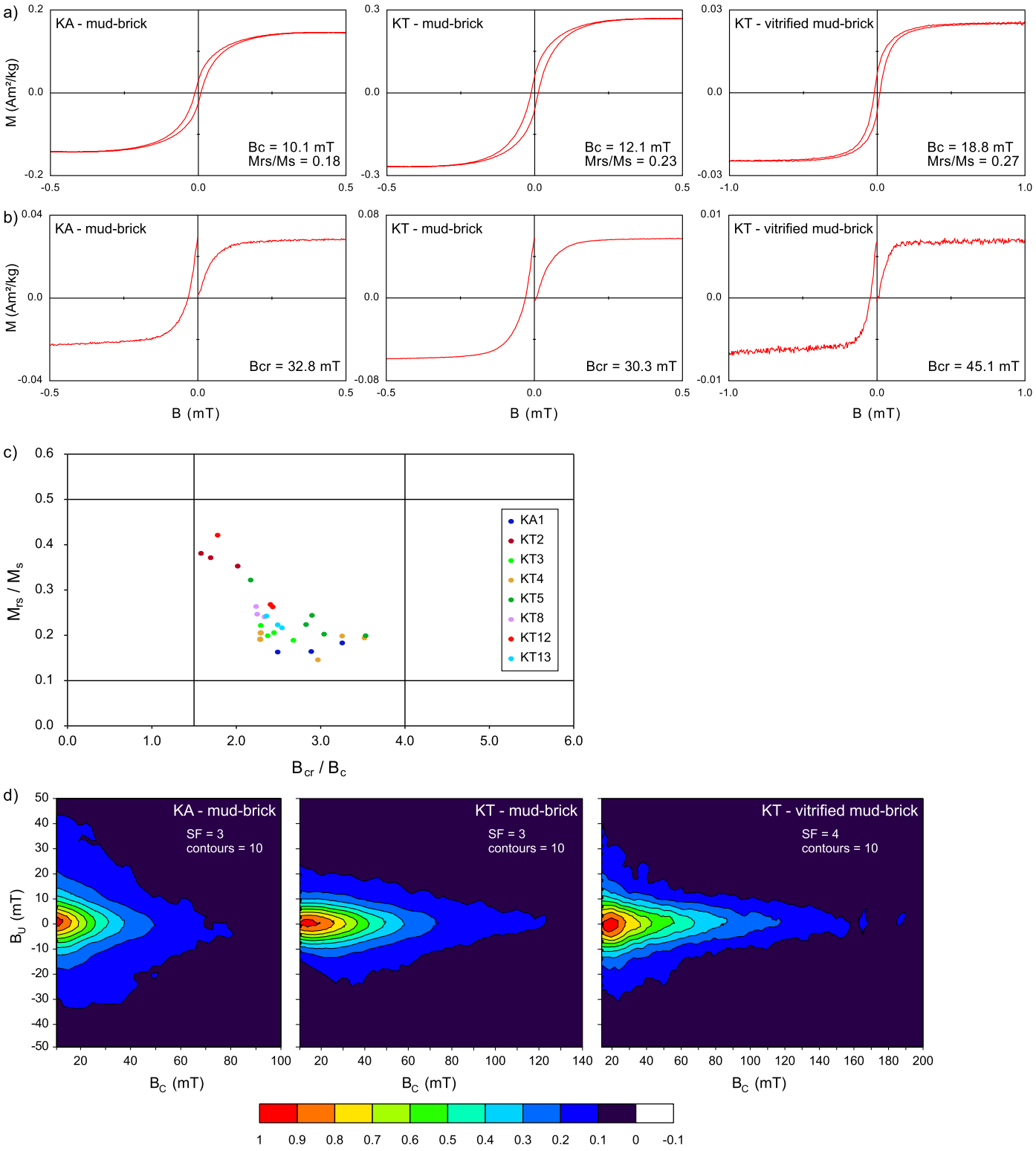

Fig. 3. (a) Hysteresis loops (displayed after the paramagnetic and diamagnetic correction on a mass-specific basis) and (b) IRM acquisition curves for three different material types: mud-bricks from KA, mud-bricks from KT and vitrified mud-bricks from KT; (c) Day Plot (Day et al., 1977) showing all magnetic mineral assemblages are composed of PSD grains; (d) representative FORC diagrams for each type of material plotted with a smoothing factor (SF) of 3 for the mud-bricks of KA and KT and SF = 4 for the vitrified mud-bricks of KT. The contour interval is taken as 10. The peak distributions are centered at +0, 10 and 20 mT respectively.

tive examples of a successful and a failed measurement from each type of experiment. These three methods were also applied to a large set of volcanics from Hawaii by De Groot et al. (2013) who concluded that the results were remarkably accurate if the results of two or more methods mutually agreed, testifying to the importance to not adhere to just one protocol.

4.1. Thermal IZZI-Thellier experiments (TT)

The experiments were performed using a laboratory field of 50–60 μT and a temperature range of 20–530 °C. The IZZI protocol (Tauxe and Staudigel, 2004) was used with field applied parallel to the NRM of the sample which enables the detection of multi-

Table 2a
Directional results from the studied sites. All directions are corrected for IGRF deviation.

Site	Treatment	n/N	at the site		at Kayseri		k	α_{95}
			Dec	Inc	Dec	Inc		
SPN1	Th, AF	9/14	4.0	56.9	4.0	55.6	118.7	4.7
KA1	Th, AF	7/8	−1.8	45.1	−1.3	44.4	1066.4	1.8
KA2	Th, AF	8/20	−7.0	56.3	−6.8	55.6	123.5	5.0
KA3	Th, AF	–	–	–	–	–	–	–
KA4	**Th, AF**	**10/11**	**15.3**	**49.8**	**15.6**	**49.7**	**64.6**	**6.1**
KT1	Th, AF	25/26	5.0	56.0	5.0	56.0	300.0	1.7
KT2	Th, AF	38/44	−11.3	50.3	−11.3	50.3	215.7	1.6
KT3	Th, AF	13/14	2.9	48.4	2.9	48.4	603.9	1.7
KT4	Th, AF	11/15	1.0	42.1	1.0	42.1	533.2	2.0
KT5	Th, AF	61/70	0.2	44.2	0.2	44.2	363.9	1.0
KT6	Th, AF	–	–	–	–	–	–	–
KT7	Th, AF	–	–	–	–	–	–	–
KT8	Th, AF	14/17	2.2	41.4	2.2	41.4	348.9	2.1
KT9	Th, AF	10/16	−6.5	57.0	−6.5	57.0	385.3	2.5
KT10	Th, AF	–	–	–	–	–	–	–
KT11	Th, AF	–	–	–	–	–	–	–
KT12	Th, AF	53/53	3.9	59.7	3.9	59.7	243.7	1.3
KT13	Th, AF	15/18	−2.6	45.9	−2.6	45.9	154.8	3.1

n/N, number of samples accepted over measured; Dec, mean declination; Inc, mean inclination; k, precision parameter; α_{95}, 95% confidence cone of mean directions. In bold are the rejected data points due to low k-value.

Table 2b
The intensity results obtained from three protocols. A is the average paleointensity value of individual samples and stdev is the standard deviation.

	TT			MW			MSP				AVERAGE PI	
	N/n	PI	stdev	N/n	PI	stdev	N/n	Protocol	PI	stdev	A	stdev
KA1	3/3	58.86	1.40	2/1	57.45	–	4/0	*rejected – alteration*			58.51	1.35
KT1	1/0	–	–	1/1	60.94	–	4/4	MSP-DB	58.23	0.03	59.58	1.92
KT2	2/1	60.37	–	2/0	–	–	–	–	–	–	60.37	–
KT3	4/3	54.92	1.16	5/5	63.08	13.31	4/4	MSP-DB	40.15	0.05	57.81	12.18
KT4	5/5	55.27	4.47	1/0	–	–	4/4	MSP-DSC	51.68	0.29	54.67	4.26
KT5	4/4	49.51	7.87	3/3	56.71	2.95	4/3	MSP-DSC	43.67	0.02	51.48	7.19
KT8	7/7	53.54	0.96	3/1	56.80	–	4/3	MSP-DB	57.22	0.00	54.31	1.75
KT12	4/4	63.83	5.17	1/1	60.60	–	4/4	MSP-DB	57.66	0.07	62.26	4.78
KT13	3/3	53.38	1.38	3/2	58.20	6.30	4/3	MSP-DSC	46.92	0.03	53.91	5.10

domain behavior and benefits from the advantages of providing the opportunity to check the consistency of IZ and ZI steps and rendering an extra pTRM tail check unnecessary (Yu and Tauxe, 2005).

A custom built orientation tray was used to align each sample's NRM with the applied field direction, reducing the effects of anisotropy during TRM acquisition (Rogers et al., 1979). The results were interpreted using the NRM-TRM plots. The acceptance criteria, adopted from Coe et al. (1978) and supplemented by those of Selkin and Tauxe (2000), are as follows:

1. For the linear fit:
   - the number of points used for the best fit line (N) ≥ 5;
   - the ratio of standard error of the slope to absolute value of the slope (β) < 0.1
2. The NRM fraction (f) ≥ 0.4. An exception to this is specimen KT8_10 with $f = 0.35$ but where a sister specimen has $f > 0.5$. Some 70% of accepted results had $f \geq 0.55$ as recommended by Paterson et al. (2015)
3. Quality factor (q) > 5, where most results are higher than 10
4. For the pTRM checks: (Paterson et al., 2015)
   - number of successful pTRM checks ≥ 3;
   - the ratio of difference between the pTRM check and relevant TRM value to the length of the selected NRM-TRM segment (DRAT) $< 10\%$.
5. MD behavior (i.e. 'sagging') of the interpreted segment of the NRM-TRM plot is assessed by the curvature statistic ($|k|$, Paterson, 2011 and should be <0.15, Cromwell et al., 2015).

In addition, the directional aspects such as the MAD and α were analysed by principal component analysis and the upper limits are set to 10%.

4.2. Microwave experiments (MW)

The experiments on the mud-brick samples were performed using the IZZI protocol (Tauxe and Staudigel, 2004) and a laboratory field ranging from 35–100 μT, applied at least 45 degrees from the NRM direction. Possible influence of anisotropy was checked for by comparing the direction of the magnetization acquired with that of the applied field. In all cases, no significant systematic offsets were observed suggesting that anisotropy was negligible. For three specimens from the sherds, the IZIZ protocol was used with laboratory field parallel to the samples NRM (Aitken et al., 1988; Walton, 1979). In both protocols, to check for possible influence of thermo-chemical alteration, pTRM checks were performed after every two double-treatments. The same selection criteria were employed as in the TT experiments.

4.3. Multi-Specimen Method (MSP) corrected for domain state (DSC)

To reduce the effect of non-ideal MD behavior and progressive alteration during TT experiments, Dekkers and Böhnel (2006) proposed a method, the 'multi-specimen parallel differential pTRM method', here referred to as MSP-DB. The idea behind the method is simple: to overprint an ancient TRM with a laboratory pTRM induced at a temperature much lower than the Curie temperature in a laboratory field applied in the same direction as the TRM. The initial suggestion that this protocol was domain-state in-

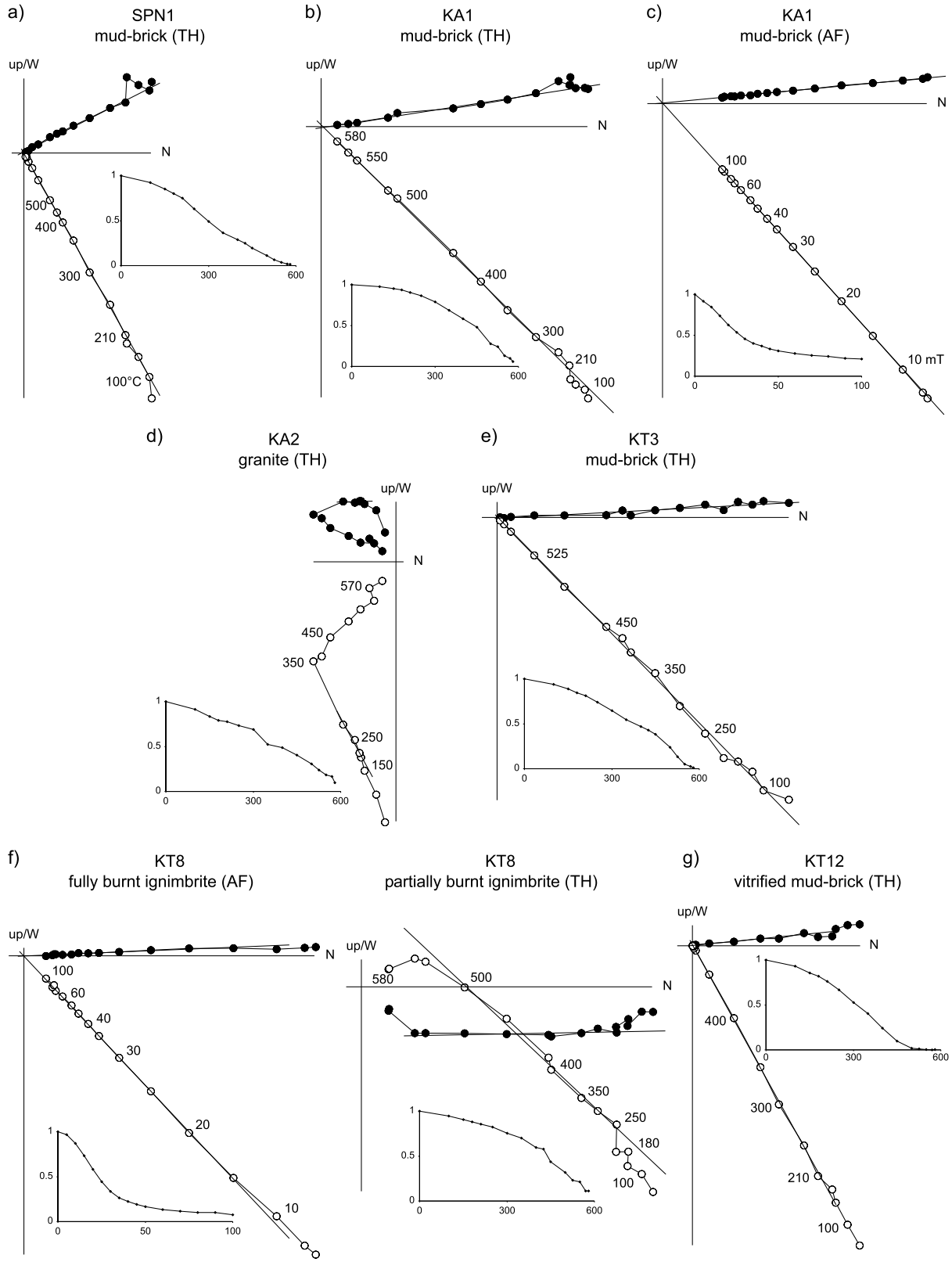

Fig. 4. Representative examples of demagnetization diagrams from each type of material. Closed (open) symbols are the projection of the vector end-points on the horizontal (vertical) plane. The corresponding temperature (in °C) or the alternating field (in mT) values are shown. In parentheses the method used to demagnetize the sample. Normalized intensity decay plots are also shown on either side of the demagnetization diagram. (a) Single component magnetite magnetization from the mud-bricks of SPN; (b, c) Th/AF demagnetization diagram of single component magnetite magnetization from the mud-bricks of KA with possible contribution of maghemite; (d) two component (LT and HT) demagnetization diagram from the granites of KA; (e) single component demagnetization diagram from the mud-bricks of KT; (f) single component and two component demagnetization diagrams from the ignimbrites of KT; (g) uniformly decaying single component demagnetization diagram from the vitrified mud-bricks of KT.

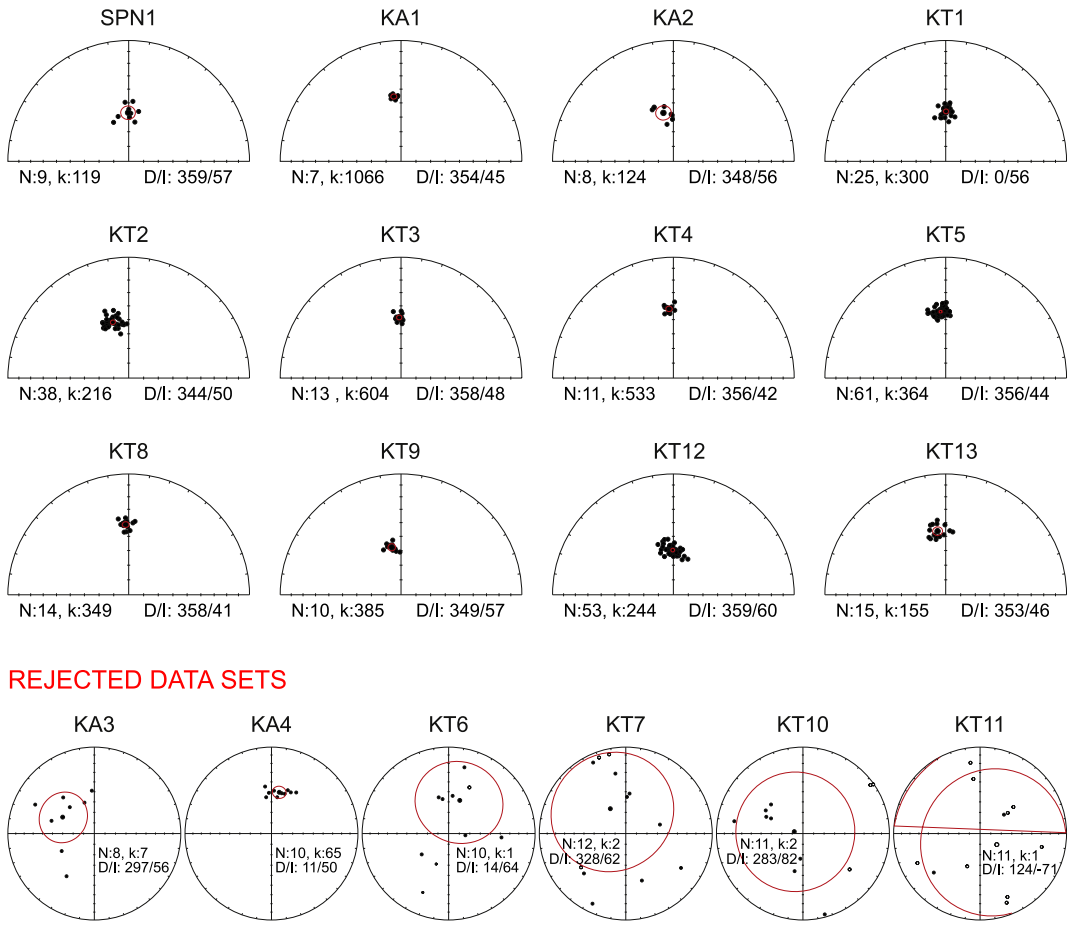

Fig. 5. Equal area projections of the characteristic remanent magnetization direction of each set. The red circles are α_{95} cones of confidence. N is the number of samples, k is precision parameter, and D/I is the declination/inclination. Below are the rejected data sets due to low k or high α_{95} value. (For interpretation of the references to color in this figure legend, the reader is referred to the web version of this article.)

dependent, however, did not hold; Fabian and Leonhardt (2010) proposed an addition to the protocol to correct for MD behavior. As a rule, we apply the domain-state corrected protocol, referred to as MSP-DSC.

To conduct the MSP-DB and MSP-DSC measurements we used four specimens per site, simply because there were insufficient specimens. For the MSP experiments, it is first necessary to check for the absence of secondary magnetizations, and then to select a set-temperature for the pTRM acquisition that is below the point where chemical alteration is significant. To determine this temperature we relied on the a priori knowledge from the rock magnetic experiments and the thermal demagnetization. The experiments were conducted using thermal demagnetiser. To induce the pTRM parallel to the NRM, we used a specially designed sample holder. Because of the limited amount of specimens we applied 4 steps. The samples were heated at either 300 or 350 °C. The MSP experiments were accepted if the average progressive alteration, $\varepsilon_{\text{alt}} < 3\%$. When $\varepsilon_{\text{alt}} > 3\%$, the data point with the highest alteration is omitted from the group. If the average alteration after the omission is less than 3%, the new best fit and its error envelopes are calculated based on three data points. For the MSP-DCS protocol there is an additional requirement where, Δb, the difference between the theoretical ($b = -1$) and the actual value of y-axis intercept of the best-fit line should be smaller than 10%. If this requirement was not fulfilled, implying that the MSP-DSC protocol did not properly correct for MD behavior, we used the MSP-DB protocol provided that the ε_{alt} is still less than 3%.

5. Results

5.1. ChRM directions

Şapinuva. The samples that are collected from the fallen mud-bricks (SPN1) show single component magnetite magnetizations (Fig. 4a). There is a slight inflexion in the thermal decay curve at ∼350 °C. This observation is coherent with what was found in the Curie curves (Fig. 2) and could imply that there could be maghemite. Out of 14 samples, 5 samples (two being sister samples) gave inconsistent directions, indicating that the mud-brick blocks from which they were sampled were displaced after burning. When these 5 samples are discarded, the distribution becomes clustered with $k > 100$ (Fig. 5, Table 2a).

Kalehöyük. The samples from KA produced good results from its mud-bricks (Fig. 4b, c) and less conclusive or no result from the granites (Fig. 4d). Clearly, the granites have not been fully heated. The set from KA1 is composed solely of mud-bricks. The demagnetization diagrams are single component with a minor overprint removed at low temperatures (Fig. 4b). The remanence is nearly completely removed at 580 °C but not yet at 100 mT, which could indicate the presence of some maghemite. In the AF demagnetization diagrams, the percentage of remanence that is left after 100 mT is ∼20% (Fig. 4c). From 8 cores measured, 7 gave successful results producing a well-defined ChRM with high k-value of 1066.

Sampling of KA2 was made on four blocks of granite and one block of mud-brick. Out of 20 samples measured, 12 belonging to

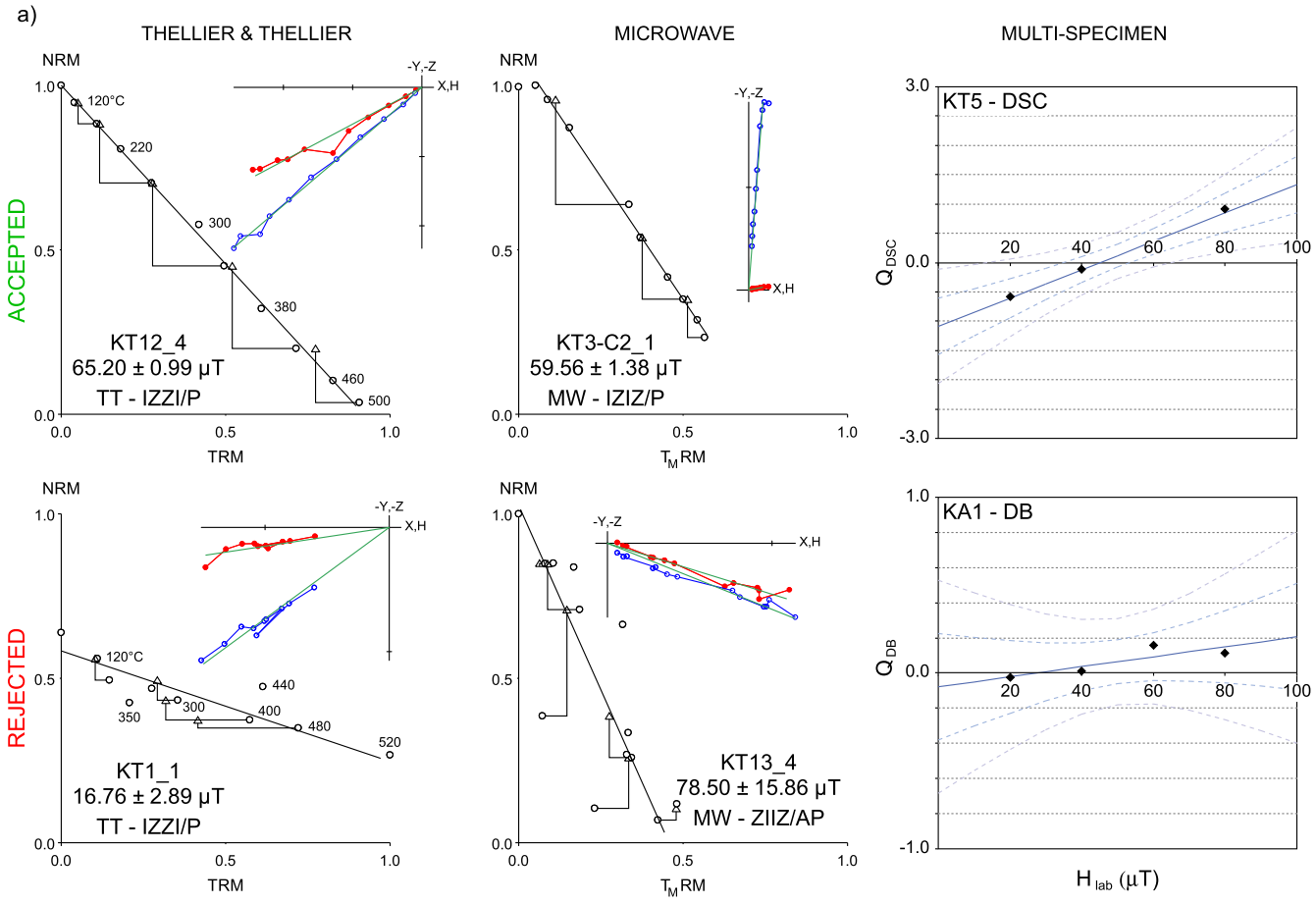

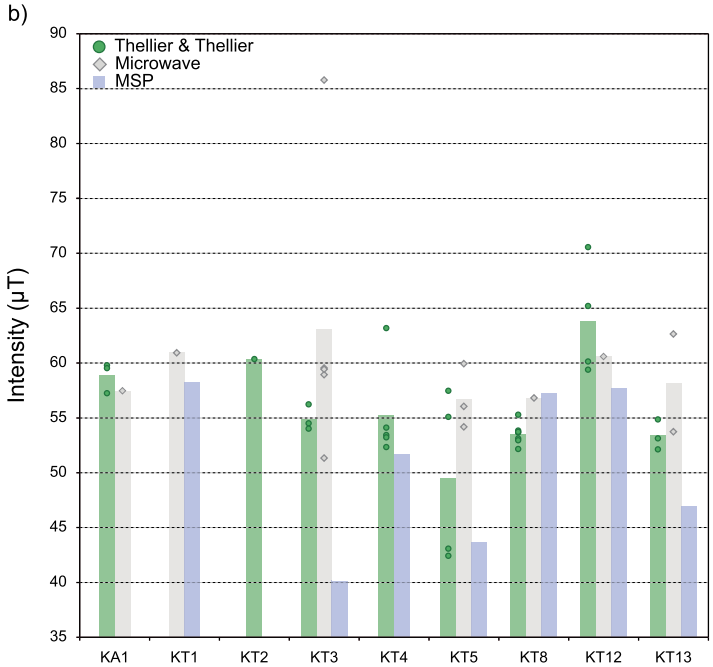

Fig. 6. (a) Representative examples of a successful and a failed measurement obtained from three different paleointensity methods. The NRM-TRM plots of a thermal IZZI-Thellier (TT) and a microwave (MW) experiment are shown with associated orthogonal vector plots in core coordinates. Solid red (open blue) symbols are horizontal (vertical) planes. Diagrams are normalized to initial NRM intensity. The arrows represent the pTRM checks engaged in every two double-treatments. P/AP/SP stands for the applied field direction parallel/antiparallel/subperpendicular to the samples NRM. The relevant temperature steps for TT experiments are shown on the side of the data point. ThellierTool4.0 (Leonhardt et al., 2004) was used to plot the data. On the left an accepted 'domain corrected' solution (MSP-DSC) and a rejected 'parallel differential pTRM' solution (MSP-DB) of multi-specimen method are shown. (b) Comparison of the results from three different protocols. The site means are shown as histograms and the individual measurements are represented in diamonds and circles. (For interpretation of the references to color in this figure legend, the reader is referred to the web version of this article.)

two different granite blocks produced single component magnetization diagrams with random – likely original – directions indicating that they were not burnt at sufficiently high temperatures. The samples from the other two granite blocks have a low-temperature (LT) due to partial heating (Fig. 4d) up to some 350 °C and a high-temperature (HT) randomly directed component, whereas the mud-brick samples are single component. The ChRM analysis of these three blocks, where mud-bricks are in agreement with the LT component of granites, yields a cluster with $k > 100$.

The samples collected from KA3 have single component demagnetization diagrams with random groups of directions indicating that the granite blocks carry their original magnetizations and hence were not sufficiently burnt (Fig. 5). This is in line with the results from the calculation of Q_n where the majority of the granites have $Q_n < 1$ (Fig. 2a).

The set from KA4 is also composed of only granites collected from two different blocks from the foundation of a mud-brick wall where KA1 was taken. The demagnetization diagrams are generally single component but of low quality. In some samples, there is a slight inflexion in the decay curve ~500 °C which can be interpreted as a second magnetic mineral. The fact that there is an inflexion in the decay curve at that temperature, but no obvious bending in the Curie curves suggests that the reason is insufficient burning rather than a second magnetic mineral (Figs. 2, 4). The ChRM of the set displays a poor cluster with $k = 64$, $\alpha_{95} = 6.1$ and there is significant disagreement between the directions obtained from KA1 and KA4. Considering the scattered distribution of KA4, the granite blocks may have slightly moved (Fig. A3) while the mud-brick wall (KA1) is more solid and better burnt. Therefore, the results from KA1 are considered to be more reliable and directions from KA4 are discarded from further analyses (Fig. 5, Table 2a).

Kültepe. The samples collected from Kültepe generally produced good results, especially from the mud-bricks. The sets that are composed solely of mud-brick (KT1, KT2 and KT3) show single component magnetite magnetization with a minor overprint that is completely removed at low temperatures (Fig. 4e). This is supported with the findings from the Curie curves where the mud-bricks display an ideal magnetite magnetization and the uniform thermal decay (Figs. 2, 4e). These three sets have well-defined ChRMs with high k values (200–600) and $\alpha_{95} < 1.7$.

Out of 5 sets that are composed only of ignimbrites, 4 sets (KT6, KT7, KT10 and KT11) have turned out to be not sufficiently burnt considering the single component demagnetization diagrams with random directions (Fig. 5). The samples from the last ignimbrite set, KT9, were either fully burnt providing a meaningful direction or sufficiently heated to have a clear well-determined LT component in the demagnetization diagram that we consider to represent a ChRM due to firing. This set is also of good quality with $k > 300$, $\alpha_{95} < 2.5$.

There are 4 sets (KT4, KT5, KT8 and KT13) that are composed of both mud-bricks and ignimbrites. The ignimbrite samples from these sets have either single or two component demagnetization diagrams (Fig. 4f) whereas the mud-bricks are single component. The directions obtained from these two different building materials (the LT component of ignimbrites) are consistent within each set. Only 2–3 samples in each set were clear outliers (ignimbrites, obviously not sufficiently heated) and therefore excluded.

There is one set that is composed fully of vitrified mud-bricks (KT12). The demagnetization diagrams are single component decaying uniformly straight to the origin (Fig. 4g). The Curie curves represent an almost purely paramagnetic contribution (Fig. 2) and did not allow identification of the magnetic carrier. The demagnetization diagrams, however, show that the magnetization is fully removed at ~500 °C pointing to Ti-poor magnetite. The set displays a well-defined ChRM with $k = 244$, $\alpha_{95} = 1.3$ (Fig. 5, Table 2a).

Out of the 13 sets of samples from Kültepe, 9 are considered to be of good quality with IGRF corrected declinations between 348.7° and 5.0° and inclinations between 41.4° and 59.7°.

5.2. Archaeointensity results

Archaeointensities were determined for 9 sets of samples (1 set of mud-bricks from KA, 1 set of vitrified mud-bricks from KT and 7 sets of mud-bricks from KT) where 5 were successful to yield a result in all three methods. Fig. 6a shows an example of a successful and a failed measurement from each method. The plots of all measurements are presented in Figs. A5 and A6, results are reported in Table 2b and detailed statistical parameters are given in Tables A2 and A3. The results from different protocols reasonably agree with each other, yet, except for KT8, the MSP results are systematically lower than the other two protocols (Table 2a, Fig. 6b). This discrepancy is the highest in KT3 (up to 35% with the MW). Out of 54 TT and MW measurements, 44 are appointed to be successful (Table A2). From 8 sets of MSP measurements, 7 were successful either with DSC or DB solution. No systematic differences were observed between the TT and MW results from the same sample sets. Since the cooling rate effect, if present, is expected to be enhanced in MW estimates and make them systematically higher than sister estimates using longer cooling times (Poletti et al., 2013), this agreement suggests that no cooling rate correction is required for the data as a whole. Moreover, the remanence in our samples is predominantly carried by PSD grains (Figs. 3c, d) for which the cooling rate effect on (p)TRM magnitude has been experimentally verified as small (e.g. Yu, 2011; Biggin et al., 2013; De Groot et al., 2013) though not necessarily negligible (Chauvin et al., 2000; Genevey and Gallet, 2002; Genevey et al., 2003; Gomez-Paccard et al., 2006; Osete et al., 2015).

The set from the mud-bricks of KA1 has a mean intensity value of 58.5 μT from 3 TT (out of 3) and 1 MW (out of 2) measurements. The single successful MW measurement is in excellent agreement with the TT measurements where the result differs by 1.4 μT from the TT average. The MSP results were rejected due to alteration.

From KT1, we made one TT measurement which has failed and one MW measurement with intensity value of 60.9 μT in which the MSP-DB result (58.2 μT) obtained from four data points is in line with the value within 5%.

The samples from KT2 and KT4 produced good quality TT results, however, failed in all MW experiments either due to noisy NRM-TRM plot, indestructible NRM or MD-curvature (KT2_3, KT2_4 and KT4_6, respectively, in Fig. A5). We were not able to perform the MSP method on KT2 because there were not enough samples, so we present an intensity value of 60.4 μT for the set, based on one TT measurement. The MSP result from KT4 is of good quality with minor alteration and $\Delta b < 10\%$ allowing to opt for the domain corrected solution. The set has a mean intensity value of 54.7 ± 4.3 μT based on 5 TT and an MSP-DSC result derived from four points.

The majority of TT & MW (22/21 TT, 15/12 MW) measurements from the sets KT3 (mud-bricks and sherds), KT5, KT8, KT13 (mud-bricks) and KT12 (vitrified mud-bricks) have passed the selection criteria, producing high quality NRM-TRM plots. The TT and MW measurements from the mud-bricks of KT3 produced comparable results whereas the MSP result is approximately 30% lower than the average of these two methods. The samples from KT5 produced two low and two high TT results in which the lower values are in line with the MSP-DSC result and the higher values are in agreement with the MW. The set has a mean intensity value of 51.5 ± 7.2 μT. Among all sets, KT8 has the most consistent results in both individual sample level and mean intensities obtained from three protocols. For the MSP measurement the average alteration

is slightly (2%) higher than the acceptance limit ($\varepsilon_{alt} = 3.06\%$), but we included the result since the data points are perfectly linear and the result is in excellent agreement with the other two protocols. Two data points from the microwave produced very similar intensity values with each other and with the other protocols, but they are discarded since they have slightly higher curvature values than the acceptance limit (both $|k|$ values are 0.16). 7 TT and 1 MW measurements, and a MSP-DB solution from three data points produced an average intensity of 54.3 ± 1.8 μT. The measurements from the vitrified mud-bricks of KT12 produced the highest intensity value with 62.3 ± 4.8 μT from 6 measurements (4 TT, 1 MW and 4 data points from MSP-DB). The set has exceptionally high f value ($f_{ave} = 0.84$) compared to other sets (Table A2). The samples from KT13 produced well behaved NRM-TRM diagrams from TT, acceptable results from the MW method. The set has a mean intensity value of 53.9 ± 5.1 μT obtained from 3 TT, 2 MW and a MSP-DSC result.

6. Discussion

6.1. ChRM directions

To be able to compare our results with the existing Eastern Europe and the Middle East data from GEOMAGIA50 and the Turkish data (Ertepinar et al., 2012; Sarıbudak and Tarling, 1993; Sayın and Orbay, 2003), they were relocated to Kayseri. Then, all the data points are plotted against the existing data from GEOMAGIA50 and geomagnetic field models calculated at Kayseri (Figs. 7a, b). We use the latest models SHA.DIF.14k (Pavón-Carrasco et al., 2014) and pfm9k.1b (Nilsson et al., 2014); both models provide error envelopes. The pfm9k.1b model uses also sediment data, and is appreciably more smoothed and has a larger error envelope than SHA.DIF.14k (Figs. 7, 8).

A first observation is that the new model SHA.DIF.14k very well fits our earlier directional observations, including the large declination swing to nearly 20°E around 2000 BCE (Fig. 7a). This swing was not recorded by the CALS7k model (Korte and Constable, 2005) we then used. Nor is it recorded by the heavily smoothed pfm9k.1b model. The new model also fit very well the directional data previously obtained by Ertepinar et al. (2012), for example the inclination values around 2500 BCE (Fig. 7b). The model only shows a less perfect fit with the paleointensities (VADM), and both our earlier data and the compiled Middle East data (Fig. 7c) are still higher than both models predict around 2600–2500 BCE.

With respect to our new data, the prediction of declination from the models agrees within error with the declination of the single direction from ~1350 BCE (**SPN1**) while the inclination value is lower (by more than 10°) than predicted. At this time interval SHA.DIF.14k shows a maximum in the inclination as high as 68°. The records from Greece (Tarling and Downey, 1990) and Turkey (Sayın and Orbay, 2003) around this period are on average 5° higher than our result. Because of the large error bar of **SPN1**, the result still falls within the range predicted by pfm9k.1b.

There are three directions from ~1765 BCE, **KT1, KT9** and **KA1**, where all three are reported to come from the same level (Kültepe Ib) with a very well constrained age, all have high k values (300–1066) and low α_{95} (1.7°–2.5°). The inclination prediction of SHA.DIF.14k is in perfect agreement with **KT1** and **KT9**. The declination of **KT1** is also in line with the model; however the declination of **KT9** is 10° to the west of the predictions but still in the error envelope of pfm9k.1b. The direction of **KA1** from the allegedly time equivalent level, however, does not fit within error with SHA.DIF.14, especially the inclination is 10° lower than predicted, while only the declination falls within the error envelope of pfm9k.1b. In this interval the Turkish data (Sayın and Orbay, 2003) show a large swing in declination, up to 25° to the east compared to the models. This shallow inclination of **KA1** can be explained by either an overprint of another fire event occurring in a later stage of the settlement, or the assumed age for the level (Kültepe Ib, 1765 BCE) is not correct. This assumption is discussed in more detail in section 6.3.

The data sets from 1892.5 ± 57.5 BCE (**KA2, KT2, KT3, KT4, KT5, KT8,** and **KT13**) show a wide range of declination (348.7°–2.9°) and inclination (41.4°–55.6°) values, in a short time interval of ~115 years. The declination results are mostly consistent with pfm9k.1b, but with respect to SHA.DIF.14k most declinations are significantly (0–12°) to the west of the prediction. The inclinations are partly within range and partly shallower, up to 7° with respect to SHA.DIF.14 and 15° with respect to pfm9k.1b, but consistent with the GEOMAGIA50 data from Greece, which admittedly are very few. Naturally, it is inevitable that the models are heavily smoothed and cannot adequately represent such rapid variations, but it is noteworthy that around 1875 BCE, SHA.DIF.14k shows a significant dip in inclination. The relative ages of these data points are discussed in more detail below.

The oldest site from Kültepe (**KT12**, ~2400 BCE) produced a high quality result with directions in agreement only with pfm9k.1b model, but not with the curves derived from SHA.DIF.14k.

These new results are very useful to improve the resolution of the models since there is lack of directional data for this time period. Only 8 records are available in GEOMAGIA50 for the 700 year long period 2200–1500 BCE, from Greece to Azerbaijan, and from Moldavia/Ukraine to Egypt. Our 10 (out of 12) new directional records in this time interval plus the 3 results from Ertepinar et al. (2012) almost triple the database for this entire region. In addition, these high quality data sets contribute in terms of a better spatial distribution. This will reduce any bias (the local variations in the field) introduced by the few existing data sets, considering that the majority of the GEOMAGIA50 data is coming from Eastern Europe, some from the Near East (22%) and very few from the Middle East (only 2%).

6.2. Archaeointensities

All the archaeointensity values were converted into virtual axial dipole moments (VADM) and plotted along with the Middle East data (see introduction for references related to Levant), Turkish data (Ertepinar et al., 2012), GEOMAGIA50 data within a circle of ~1600 km from Kültepe (38.85°N and 35.63°E) and the global field models SHA.DIF.14k and pfm9k.1b (Fig. 7c). A summary of the palaeointensity results are in Table 2b, while all details can be found in Tables A2, A3.

The data sets from $\sim 1765 \pm 65$ BCE, **KA1** and **KT1** produced similar intensity values, higher than the prediction of both models and the majority of the Middle East data. The fact that at least two different methods involved in the acquisition of the results (TT + MW for **KA1** and MW + MSP for **KT1**) produce the same intensity however, gives faith that these higher intensities are reliable. There are several very similar intensities in this same period from Ben-Yosef et al. (2008a) and from GEOMAGIA50: two results from Bulgaria are identical within error. Hence there seems to be a short period of high intensities ~1765 BCE. Additional measurements from these levels would increase the reliability of the data points.

The intensity values of data sets from 1892.5 ± 57.5 BCE (**KT2, KT3, KT4, KT5, KT8 and KT13**) show a dispersion of <9%, the highest being 10.55×10^{22}, and the lowest 9.00×10^{22}. These palaeointensities are higher than the prediction of SHA.DIF.14k, GEOMAGIA50, and Middle East data, although there are a few results from Syria, Greece and Egypt that are in line with our results within the age uncertainties.

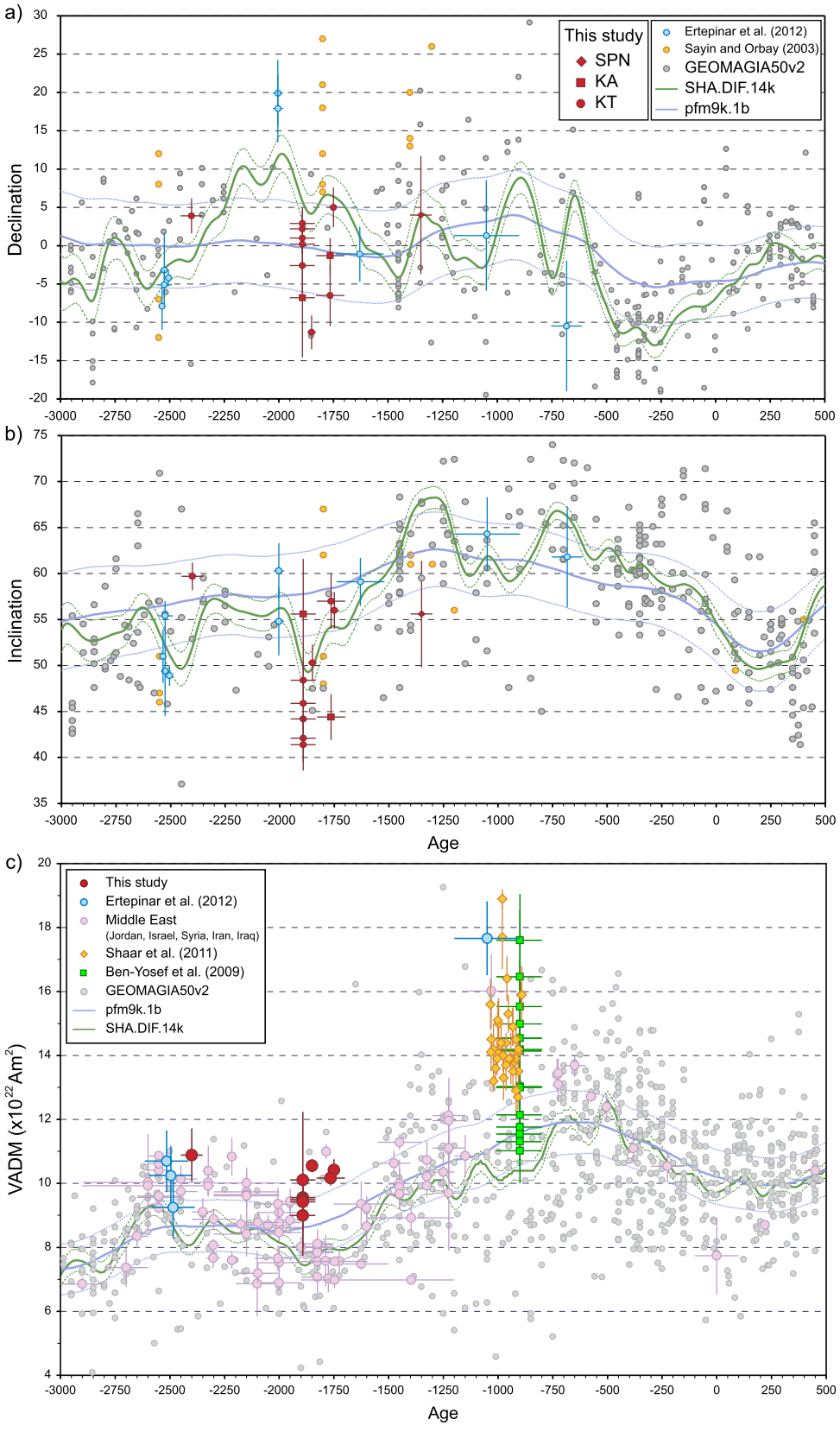

Fig. 7. Comparison of (a) inclination and (b) declination results of this study (red) with the Eastern Europe and Near & Middle East archaeomagnetic data from GEOMAGIA50v2 (gray), the Turkish data (orange and blue), and the global geomagnetic field models pfm9k.1b and SHA.DIF.14k; (c) mean site VADM values of this study (red) plotted against the data from GEOMAGIA50v2 (gray), Middle East (pink circles, orange triangles and light green squares), Turkey data (blue circles) from Ertepinar et al. (2012) along with the two global geomagnetic field models. All data are recalculated to Kayseri (see caption to Fig. 1). (For interpretation of the references to color in this figure legend, the reader is referred to the web version of this article.)

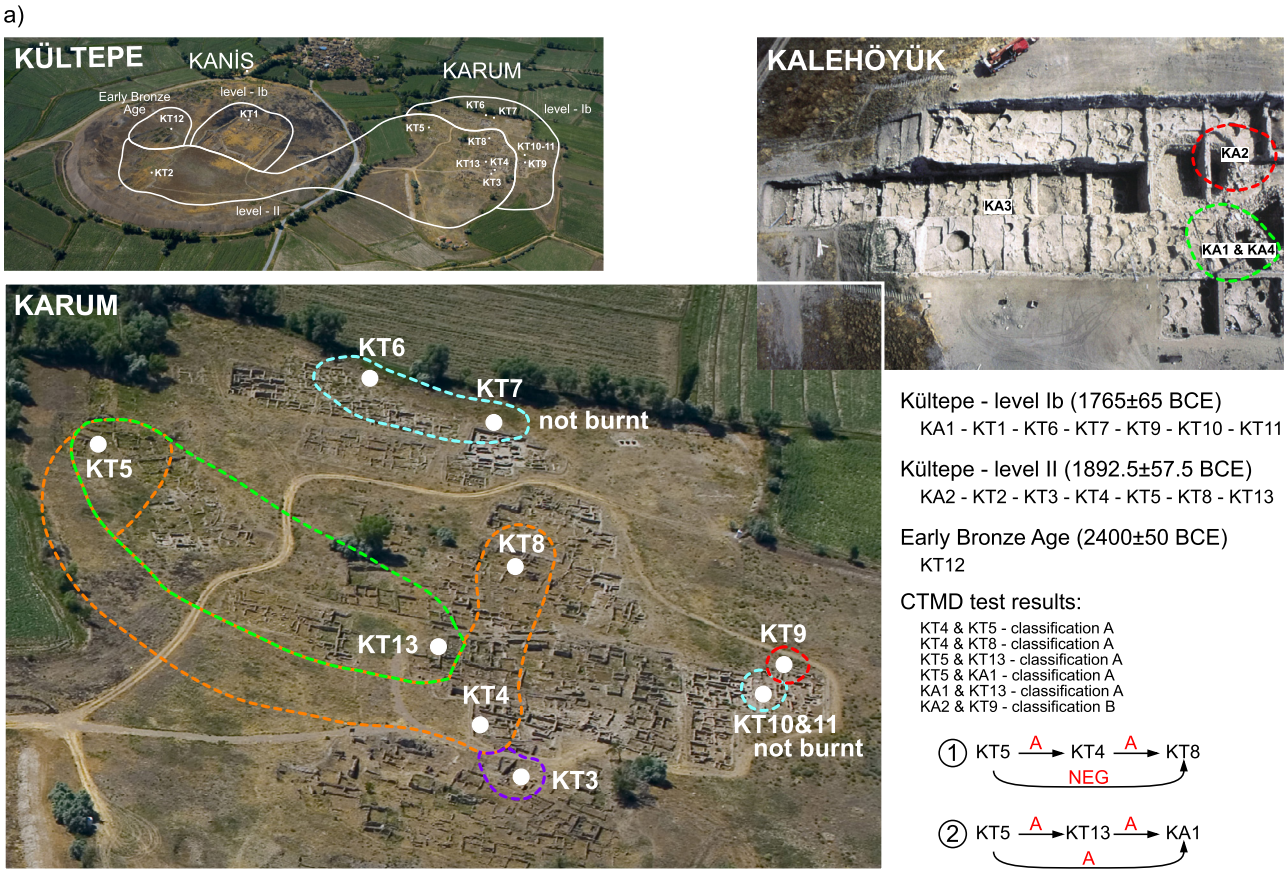

Fig. 8. (a) Areal distribution of fire events shown on an aerial photograph of site Kültepe; (b) declination, inclination and VADM distribution of Kültepe level II data points (green dots) as sorted from the most westerly to the most easterly declination based on the westerly trend in the SHA.DIF.14k model for the period of ~2100–1850 BCE. The blue dots are data points from Kültepe-level Ib and the black dots are Turkey data from Ertepinar et al. (2012). The time intervals between sites in Kültepe-level II are arbitrarily taken as 20 years. (For interpretation of the references to color in this figure legend, the reader is referred to the web version of this article.)

The archaeointensity result ($10.89 \pm 0.84 \times 10^{22}$ Am^2) from the data set from ~2400 BCE (**KT12**) is also significantly higher than what is predicted by the models and the GEOMAGIA50 data. However, this high intensity could fit very well with the high intensity interval (2600–2450 BCE) found in both the Middle East and Turkey.

Our data from the period 2600–1700 BCE (including those of our earlier study) are always significantly higher than predicted by the SHA.DIF.14k model based on archaeomagnetic and lava flow data, and generally higher than predicted by pfm9k.1b (Fig. 7c) but they are not in disagreement with published data (e.g. Ben-Yosef et al., 2009; Shaar et al., 2011; Ertepinar et al., 2012) that support the existence of short-lived periods with high intensities, at least as observed in the Levant.

6.3. Relative chronology of fire events in the Assyrian Trade Colony Period sites

We have analysed the directional results of the KT sites to determine if they can be attributed to the same distribution or not. This allows us to assess whether the fire events in Kültepe belong to a single big catastrophic event or to different (temporal) events. We used the common true mean direction (CTMD) test developed by McFadden and McElhinny (1990), performed with Monte Carlo simulation for effectively applying the V_w statistic test (Watson, 1983). This test gives the angle (γ) between the means, and γ_c, the critical angle in the test is determined. If $\gamma < \gamma_c$ the test is positive and the distributions share a CTMD. The test is classified as A, B, C or indeterminate, depending on the value of γ_c. We used also the approach of Tauxe (2010), where we performed a bootstrap on the actual data points in our distributions rather than the parametric bootstrap used in the V_w statistic test. We then compare the cumulative distributions of the cartesian components of the bootstrapped means and their 95% error bounds (Tauxe, 2010). This is a better approach for small data sets and does not require the data set to have a prescribed (e.g. Fisherian) distribution. In our case, all CTMD results using both approaches were identical, be it that the non-parametric ('simple') bootstrap does not provide a classification.

The sets KT4 & KT5, KT4 & KT8 and KT5 & KT13 share a CTMD with classification A ($\gamma_c < 5°$). The rest of the correlations are negative. Furthermore, the sites from Kalehöyük are also examined for their CTMD to compare if any of the fires in this settlement is contemporaneous with any of the fire events in Kültepe. The CTMD test of the site KA2 produced a class B correlation with KT9 whereas KA1 and KT5 & KT13 share a CTMD with classification A. These latter results introduce a conflict since KT5 and KT13 are from Kültepe-level II group, and the age of KA1 is supposed to be time equivalent of Kültepe-level Ib whereas KA2 is reported to be time equivalent of Kültepe-level II and set KT9 is from Kültepe-level Ib. This disagreement is discussed in more detail in the following parts. Based on the results of the CTMD test of Kültepe-level II, the areal distribution of fires is plotted in Fig. 8a. As can be seen from the figure, KT2, KT3 and KT9 are local fires whereas KT4 & KT8 and KT5 & KT13 are larger scale fires. Therefore, we can conclude that the timing of fires in Kültepe are different and the site was not abandoned as a result of a big catastrophic fire event as was also suggested by Sagona and Zimansky (2009).

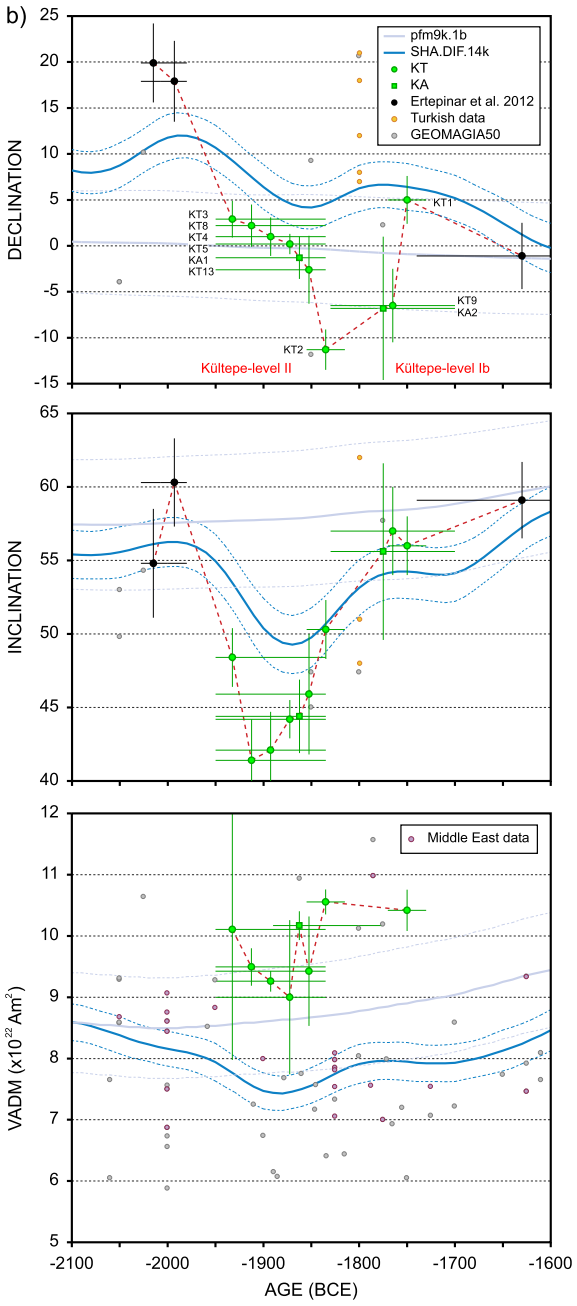

Fig. 8. (*continued*)

To establish a relative chronology for the fire events in Kültepe-level II (KT2, KT3, KT4, KT5, KT8, KT9, KT13 from Kültepe and KA2 from Kalehöyük), we sorted the data based on their CTMD results and then on easternmost to westernmost declination. This best reflects the trend in the SHA.DIF.14k model at this time interval (Fig. 8b). In this scenario, the oldest/youngest age – within the age errors – is assigned to the most westerly/easterly declination while the time span between each fire event is arbitrarily divided into equal time intervals of 20 years. The corresponding inclination values agree fairly well with the trend of the model but in this scenario declinations are more westerly towards ∼1850 BCE while inclinations are steepest around 1900 BCE. Although we have 'smoothed' the directional changes by shifting the results within the time span allowed by the dating error, it seems that the model has not (yet) enough resolution to predict these short-term swings in directions. The magnitude and timing of these swings are however compatible with observations of secular variation over the past 3000 yr.

This works well for the KT samples and provides a reasonable sequence in geomagnetic field changes. It does not work for the KA samples, however: the positions of KA1 (assumed to belong to Kültepe-level Ib) and KA2 (assumedly Kültepe-level II) do not fit at all if we retain their assumed age levels. Retaining these leads to very big and unreasonable jumps in directions at extremely short time scales, not observed in existing (historical, archaeological) secular variation records. We can only arrive at a reasonable scenario in directional changes if we assign KA2 to Kültepe-level Ib and KA1 to level II (Fig. 8b).

The VADM trend is not helpful in discriminating the best possible sequence since values are very similar. They are essentially in accordance with the trend of the curve from the SHA.DIF.14k model but systematically higher, and they are largely in agreement with pfm9k.1b. Nevertheless, the scenario preferred here represents the most reasonable sequence of fire events at Kültepe, where the rate of directional variations is similar to secular variation as observed today. We do realise however that other scenarios are possible, and that the time constraints within the given age uncertainty do not allow this – or any other – scenario to be robust. For example, a scenario in which the data sets are sorted on increasing inclinations based on the mild increasing trend in the model, results in more abrupt changes compared to the first scenario, and the declinations display erratic jumps of 5–15° within 10 year time intervals.

We favour the scenario outlined above (Fig. 8) in which both declination and inclination change gradually and abrupt and unlikely erratic changes in the directions in such a short time interval are avoided.

7. Conclusions

This study concentrated on the characterization of the full vector magnetic field over Anatolia for Assyrian and Hittite periods. The rock magnetic properties derived from room temperature susceptibilities and Curie curves for the directional analyses and additional hysteresis parameters, IRM acquisition and FORC diagrams for the intensity experiments show that the samples are suitable for archaeomagnetic experiments.

The ChRMs obtained (12 out of 18) gave good quality results with $k > 100$ and $\alpha_{95} < 5$ (Table 2a). The remaining 6 sets are either displaced or not sufficiently burnt. Together with our earlier results, we nearly triple the amount of directional results in the period 2200–1500 BCE for the entire region.

The archaeointensity experiments were carried out on 9 sets of samples using three different methods – thermal IZZI-Thellier, microwave, and the multi-specimen technique – and they produced comparable results (Table 2b). Yet, the majority of the MSP results are systematically lower than the other two protocols except in KT8. Out of these 9 sets, 5 were successful in yielding a comparable result in all three methods, a success rate of more than 50%.

The results are compared with the existing data from the region and with the global geomagnetic field models pfm9k.1b and SHA.DIF.14k. It appears that pfm9k.1b is over smoothed and has a large error envelope that accommodates most of the data presented here, with the exception of some of the palaeointensity results. The SHA.DIF.14k model is in better agreement with the directional data of this and our earlier study. The palaeointensities we find however are invariably higher than the predictions of this model.

Finally, we assess the relative order of fire events in Kültepe with the help of the field models and the CTMD test and propose that the timing of fire events are different and the abandonment of the site was not result of a single catastrophic fire event.

Acknowledgements

We would like to thank late Prof. Dr. Kutlu Emre for her valuable feedback about the site Kültepe. We are also grateful to people in the excavation teams who were helpful at all times. Particular thanks are due to Nuretdin Kaymakcı, the drilling expert on fragile archaeological material. Yael Engbers enthusiastically performed a number of MW and MSP measurements, both in Liverpool and Utrecht, for her BSc thesis.

Appendix A. Supplementary material

Supplementary material related to this article can be found online at http://dx.doi.org/10.1016/j.epsl.2015.11.015.

References

Aitken, M.J., Allsop, A.L., Bussell, G.D., Winter, M.B., 1988. Determination of the intensity of the Earth's magnetic field during archaeological times: reliability of the Thellier technique. Rev. Geophys. 26, 3–12.

Ben-Yosef, E., Ron, H., Tauxe, L., Agnon, A., Genevey, A., Levy, T.E., Avner, U., Najjar, M., 2008a. Application of copper slag in geomagnetic archaeointensity research. J. Geophys. Res., Solid Earth 113 (8).

Ben-Yosef, E., Tauxe, L., Levy, T.E., Shaar, R., Ron, H., Najjar, M., 2009. Geomagnetic intensity spike recorded in high resolution slag deposit in Southern Jordan. Earth Planet. Sci. Lett. 287 (3–4), 529–539.

Ben-Yosef, E., Tauxe, L., Ron, H., Agnon, A., Avner, U., Najjar, M., Levy, T.E., 2008b. A new approach for geomagnetic archaeointensity research: insights on ancient metallurgy in the Southern Levant. J. Archaeol. Sci. 35 (11), 2863–2879.

Biggin, A.J., Badejo, S., Muxworthy, A.R., Dekkers, M.J., 2013. The effect of cooling rate on the intensity of thermoremanent magnetization (TRM) acquired by assemblages of pseudo-single domain, multidomain and interacting single-domain grains. Geophys. J. Int. 193, 1239–1249.

Bucha, V., Mellaart, J., 1967. Archaeomagnetic intensity measurements on some neolithic samples from Çatal Huyuk, Anatolia. Archaeometry 10, 23–25.

Chauvin, A., Garcia, Y., Lanos, P., Laubenheimer, F., 2000. Paleointensity of the geomagnetic field recovered on archaeomagnetic sites from France. Phys. Earth Planet. Inter. 120 (1), 111–136.

Coe, R.S., Gromme, S., Mankinen, E.A., 1978. Geomagnetic paleointensities from radiocarbon-dated lava flows on Hawaii and the question of the Pacific nondipole low. J. Geophys. Res. 83, 1740–1756.

Cromwell, G., Tauxe, L., Staudigel, H., Ron, H., 2015. Paleointensity estimates from historic and modern Hawaiian lava flows using glassy basalt as a primary source material. Phys. Earth Planet. Inter. 241, 44–56.

Day, R., Fuller, M., Schmidt, V.A., 1977. Hysteresis properties of titanomagnetites: grain-size and compositional dependence. Phys. Earth Planet. Inter. 13 (4), 260–267.

De Groot, L.V., Biggin, A.J., Dekkers, M.J., Langereis, C.G., Herrero-Bervera, E., 2013. Rapid regional perturbations to the recent global geomagnetic decay revealed by a new Hawaiian record. Nat. Commun. 4, 2727.

Dekkers, M.J., Böhnel, H.N., 2006. Reliable absolute palaeointensities independent of magnetic domain state. Earth Planet. Sci. Lett. 248 (1–2), 507–516.

Ertepinar, P., Langereis, C.G., Biggin, A.J., Frangipane, M., Matney, T., Okse, T., Engin, A., 2012. Archaeomagnetic study of five mounds from Upper Mesopotamia between 2500 and 700 BCE: further evidence for an extremely strong geomagnetic field ca. 3000 years ago. Earth Planet. Sci. Lett. 357, 84–98.

Fabian, K., Leonhardt, R., 2010. Multiple-specimen absolute paleointensity determination: an optimal protocol including pTRM normalization, domain-state correction, and alteration test. Earth Planet. Sci. Lett. 297 (1–2), 84–94.

Gallet, Y., al-Maqdissi, M., 2010. Archéomagnétisme à Mishirfeh-Qatna: nouvelles données sur l'évolution de l'intensité du champ magnétique terrestre au Moyen-Orient durant les derniers millénaires. Akkadica 131, 29–46.

Gallet, Y., Butterlin, P., 2015. Archaeological and geomagnetic implications of new archaeomagnetic intensity data from the Early Bronze high terrace 'Massif Rouge' at Mari (Tell Hariri, Syria). Archaeometry 57 (S1), 263–276.

Gallet, Y., D'Andrea, M., Genevey, A., Pinnock, F., Le Goff, M., Matthiae, P., 2014. Archaeomagnetism at Ebla (Tell Mardikh, Syria). New data on geomagnetic field intensity variations in the Near East during the Bronze Age. J. Archaeol. Sci. 42, 295–304.

Gallet, Y., Genevey, A., Le Goff, M., Fluteau, F., Ali Eshraghi, S., 2006. Possible impact of the Earth's magnetic field on the history of ancient civilizations. Earth Planet. Sci. Lett. 246 (1–2), 17–26.

Gallet, Y., Le Goff, M., 2006. High-temperature archeointensity measurements from Mesopotamia. Earth Planet. Sci. Lett. 241 (1–2), 159–173.

Gallet, Y., Le Goff, M., Genevey, A., Margueron, J., Matthiae, P., 2008. Geomagnetic field intensity behavior in the Middle East between ∼3000 BC and ∼1500 BC. Geophys. Res. Lett. 35 (2).

Genevey, A., Gallet, Y., 2002. Intensity of the geomagnetic field in western Europe over the past 2000 years: new data from ancient French pottery. J. Geophys. Res., Solid Earth 107 (11), EPM 1-1–1-18.

Genevey, A., Gallet, Y., Margueron, J.C., 2003. Eight thousand years of geomagnetic field intensity variations in the eastern Mediterranean. J. Geophys. Res., Solid Earth 108 (5), EPM 1-1–1-18.

Gomez-Paccard, M., Chauvin, A., Lanos, P., Thiriot, J., Jimenez-Castillo, P., 2006. Archeomagnetic study of seven contemporaneous kilns from Murcia (Spain). Phys. Earth Planet. Inter. 157 (1–2), 16–32.

Korhonen, K., Donadini, F., Riisager, P., Pesonen, L.J., 2008. GEOMAGIA50: an archeointensity database with PHP and MySQL. Geochem. Geophys. Geosyst. 9 (4).

Korte, M., Constable, C., 2005. Continuous geomagnetic field models for the past 7 millennia: 2. CALS7K. Geochem. Geophys. Geosyst. 6 (2).

Leonhardt, R., Heunemann, C., Krasa, D., 2004. Analyzing absolute paleointensity determinations: acceptance criteria and the software ThellierTool4.0. Geochem. Geophys. Geosyst. 5 (12).

Livermore, P.W., Fournier, A., Gallet, Y., 2014. Core-flow constraints on extreme archeomagnetic intensity changes. Earth Planet. Sci. Lett. 387, 145–156.

McFadden, P.L., McElhinny, M.W., 1990. Classification of the reversal test in palaeomagnetism. Geophys. J. Int. 103 (3), 725–729.

Mullender, T.A.T., Van Velzen, A.J., Dekkers, M.J., 1993. Continuous drift correction and separate identification of ferrimagnetic and paramagnetic contributions in thermomagnetic runs. Geophys. J. Int. 114 (3), 663–672.

Nilsson, A., Holme, R., Korte, M., Suttie, N., Hill, M., 2014. Reconstructing Holocene geomagnetic field variation: new methods, models and implications. Geophys. J. Int. 198, 229–248.

Osete, M.L., Catanzariti, G., Chauvin, A., Pavón-Carrasco, F.J., Roperch, P., Fernández, V.M., 2015. First archaeomagnetic field intensity data from Ethiopia, Africa (1615 ± 12 AD). Phys. Earth Planet. Inter. 242, 24–35.

Paterson, G.A., 2011. A simple test for the presence of multidomain behavior during paleointensity experiments. J. Geophys. Res., Solid Earth 116 (10).

Paterson, G.A., Biggin, A., Hodgson, E., Hill, M., 2015. Thellier-type paleointensity data from multidomain specimens. Phys. Earth Planet. Inter. 245, 117–133.

Pavón-Carrasco, F.J., Osete, M.L., Torta, J.M., De Santis, A., 2014. A geomagnetic field model for the Holocene based on archaeomagnetic and lava flow data. Earth Planet. Sci. Lett. 388, 98–109.

Poletti, W., Hartmann, G.A., Hill, M.J., Trindade, R.I.F., 2013. The cooling-rate effect on microwave archeointensity estimates. Geophys. Res. Lett. 40 (15), 3847–3852.

Roberts, A.P., Pike, C.R., Verosub, K.L., 2000. First-order reversal curve diagrams: a new tool for characterising the magnetic properties of natural samples. J. Geophys. Res. 105, 28461–28475.

Rogers, J., Fox, J.M.W., Aitken, M.J., 1979. Magnetic anisotropy in ancient pottery. Nature 277, 644–646.

Sagona, A., Zimansky, P., 2009. Ancient Turkey. Routledge, 420 pp.

Sarıbudak, M., Tarling, D.H., 1993. Archaeomagnetic studies of the Urartian civilization, eastern Turkey. Antiquity 67, 620–629.

Sayın, N., Orbay, N., 2003. Investigation of secular variations of geomagnetic field using archaeomagnetic samples obtained from Central Anatolia. İstanbul Üniv. Müh. Fak. Yerbilimleri Dergisi 16, 33–43.

Selkin, P.A., Tauxe, L., 2000. Long-term variations in palaeointensity. Philos. Trans. R. Soc., Math. Phys. Eng. Sci. 358 (1768), 1065–1088.

Shaar, R., Ben-Yosef, E., Ron, H., Tauxe, L., Agnon, A., Kessel, R., 2011. Geomagnetic field intensity: how high can it get? How fast can it change? Constraints from Iron Age copper slag. Earth Planet. Sci. Lett. 301 (1–2), 297–306.

Stillinger, M.D., Feinberg, J.M., Frahm, E., 2015. Refining the archaeomagnetic dating curve for the Near East: new intensity data from Bronze Age ceramics at Tell Mozan, Syria. J. Archaeol. Sci. 53, 345–355.

Tarling, D.H., Downey, W.S., 1990. Archaeomagnetic results from Late Minoan destruction levels on Crete and the Minoan Tephra. In: Thera and the Aegean World III.

Tauxe, L., 2010. Essentials of Paleomagnetism. Univ. of California Press, Berkeley.

Tauxe, L., Staudigel, H., 2004. Strength of the geomagnetic field in the cretaceous normal superchron: new data from submarine basaltic glass of the troodos ophiolite. Geochem. Geophys. Geosyst. 5 (2).

Walton, D., 1979. Geomagnetic intensity in Athens between 2000 BC and AD 400. Nature 277 (5698), 643–644.

Watson, G.S., 1983. Large sample theory of the Langevin distribution. J. Stat. Plan. Inference 8, 245–256.

Yu, Y., 2011. Importance of cooling rate dependence of thermoremanence in paleointensity determination. J. Geophys. Res., Solid Earth 116 (9).

Yu, Y., Tauxe, L., 2005. Testing the IZZI protocol of geomagnetic field intensity determination. Geochem. Geophys. Geosyst. 6 (5).